Main Group Chemistry 20 (2021) 295–315
DOI 10.3233/MGC-210039
IOS Press

Comparative study of molecular docking, structural, electronic, vibrational and hydrogen bonding interactions on 4-hydroxy benzo hydrazide (4HBH) and its newly designed derivative [(E)–N′-((1H-Pyrrol-2-YL)methylene) – 4-hydroxy benzo hydrazide and its isomers (I, II and III)] (potential inhibitors) for COVID-19 protease

Anoop Kumar Pandey[a], Vijay Singh[b] and Apoorva Dwivedi[c,*]
[a]*K. S. Saket Post Graduate College, Ram Manohar Lohia University, Ayodhya, India*
[b]*University of Dodoma, Dodoma, Tanzania*
[c]*Department of Applied Science and Huminities, Seth Vishambhar Nath Institute of Engineering and Technology, Barabanki, India*

Abstract. Studies have shown that hydrazides and thier derivatives are used for pharmaceutical and medicinal purposes. At present, the whole world is suffering for COVID-19 virus. There are some vaccines or medicines available to treat this disease all over the world. Today the one fourth of the world's population is under lockdown condition. In this scenario, scientists from the whole world are doing different types of research on this disease. Being a molecular modeller, this inspires us to design new types of species (may be drugs) which may be capable for COVID-19 Protease. In the present effort, we have performed docking studies of title compounds with COVID-19 protein (6LU7) for anti-COVID-19 activity. A comparative quantum chemical calculations of molecular geometries (bond lengths and bond angles) of 4-Hydroxy Benzo Hydrazide (4HBH) and its newly designed derivatve [(E)-N′-((1H-Pyrrol-2-YL)Methylene) – 4-Hydroxy Benzo Hydrazide and its isomers (I, II and III)] in the ground state have also been carried out due to its biological importance and compared with the similer type of compound found in literature i.e. benzohydrazide. The optimized geometry and wavenumber of the vibrational bands of the molecules have been calculated by density functional theory (DFT) using Becke's three-parameters hybrid functional (B3LYP/CAM-B3LYP) with 6–311G (d, p) as the basis set. Vibrational wavenumbers are compared with the observed FT-IR and FTRaman spectra of 4-Hydroxy Benzo Hydrazide. TDDFT calculations are also done on the same level of theory and a theoretical UV-vis spectrum of title molecules are also drawn. HOMO-LUMO analysis has been done to describe the way

*Corresponding author: Apoorva Dwivedi, Department of Physics, Department of Applied Science and Huminities, Vishambhar Nath College of Engineering, Research and Technology, Barabanki, India. Tel.: +919415289670; E-mail: apoorvahri@gmail.com.

ISSN 1024-1221/$35.00

the molecule interacts with other species. Natural bond orbitals (NBO) analysis has been carried out to inspect the intra- and inter- molecular hydrogen-bonding, conjugative and hyper conjugative interactions and their second order stabilization energy. Nonlinear optical (NLO) analysis has been performed to study the non-linear optical properties of the molecule by computing the first hyperpolarizability. The variation of thermodynamic properties with temperature has been studied. QATIM analysis shows that hydrogen bonding occurs in 4HBH, isomer II and III respectively.

Keywords: Anti-COVID-19 activity, molecular docking, vibrational specrtroscopic analysis, DFT, HOMO-LUMO, M.E.S.P., polarizability, hyper polarizability, AIM analysis

1. Introduction

The COVID-19 virus from the family of corona emerged in December 2019 in china and then spread rapidly worldwide, particularly to China, Japan, South Korea, Italy, Spain, USA and India etc. As of march 31, 2020, a total of 803,313 confirmed cases of coronavirus disease 2019 (COVID-19) and 39033 deaths have been reported all over the world [1, 2]. Scientists are trying to find vaccines and drugs to treat this disease. In the absence of any medicine or vaccine, some antivirals including interferon α (IFN-α), lopinavir/ritonavir and chloroquine phosphate have been used for tentative treatment of COVID-19 [3]. It is seen that hydrazides have different biological activities [4–6]. Studies have shown that hydrazides and its derivatives are used for pharmaceutical and medicinal purposes [7]. Hydrazides have been known to be associated with anti-bacterial, antifungal, anthelmintic and anticonvulsant activities [8–11]. Abdulaziz et al. [12] have studied the comparative study of structures of benzohydroxamic acid (BHA) and benzohydrazide (BH). Suresh et al. [13] have done spectroscopics investigations of 2,4-dihydroxy-N′-(4-methoxybenzylidene)benzohydrazide by with experimental and theoretical aspects. A paper entitled "FTIR, FT-Raman and UV–Vis spectra of the Schiff base compound (E)-N′-(4-methoxybenzylidene) benzohydrazide (MBBH)" is also reported by Saleem et al. [14]. p-Hydroxy benzohydrazide moiety and its analogues are suitable parent compounds upon which variety of biological activities are reported such as antitumor [15], antianginal [16], antitubercular [17], antihypertensive [18] and antibacterial [19]. Suresh et al. [20] have investigated the experimental and theoretical vibrational modes of 2,4-dihydroxy-N′-(4-methoxybenzylidene)benzohydrazide. Arjunan et al. [21] have assigned and analysed the vibrational modes of benzohydrazide (BH) by using FTIR and FT-Raman spectral data. Marta Sánchez-Lozano et al. [22] have prepared the rhenium (I) carbonyl bromide complex, [ReBr(CO)3(HL)], from 2,4-dihydroxybenzaldehyde and 4 hydroxybenzoic acid hydrazide (HL). Bharty et al. [23] have synthesised two new compounds N′ [bis(methylsulfanyl) methylene]-2-hydroxybenzohydrazide {Hbmshb(1)} and N′-(4 methoxy benzoyl)-hydrazine carbodithioic acid ethyl ester {H2mbhce(2)}.

As a part of our on-going research [24–28], we have reported a camparative quantum chemical study on (E)-N′-((1H-Pyrrol-2-YL)Methylene) – 4-Hydroxy Benzo Hydrazide isomers and 4-Hydroxy Benzo Hydrazide in the ground state by using combination of DFT /B3LYP/CAM-B3LYP theory and 6–311G (d, p) as the basis set and compared with the similer type of compound found in literature i.e. benzohydrazide [29]. This DFT study on these compounds most likely help researchers to understand some modification in chemical reaction such as oxidation/reduction which generate new binding reactive sites. We have also performed molecular docking of title compounds. In this paper NLO properties of these compounds are reported for the first time which helps to explore its various NLO applications [30, 31].

1.1. Experimental details and computational methods

Geometry optimization have been done using Gaussian 03 [32] and Gauss View molecular visualization program pakages [33]. The molecular structure of the title compounds in ground state (in

gas phase) were optimized by DFT/B3LYP [34, 35] and CAM-B3LYP [36] methods with 6–311 G (d, p) as the basis set. B3LYP, the most attractive and well known DFT functional, uses Becke's 3 parameter exchange correlation functional which embrace 3 parameters to mix in the exact Hartree–Fock (HF) exchange correlation and Lee Yang and Parr (LYP) correlation functional that refurbish dynamic electron correlation. The CAM-B3LYP functional laid down by Tawada et al. consolidates the long-range correction and the hybrid qualities of B3LYP. We have used density functional theory with B3LYP and CAM-B3LYP as the basis sets. As B3LYP is most successful functional so far while CAM-B3LYP combines the hybrid and long range correlation. CAM-B3LYP performs well for charge transfer excitations which B3LYP underestimates enormously. So we have used these both basis sets for our calculation. These optimized geometry was used in the vibrational frequency calculations. Harmonic modes were multiplied by the factor 0.9614 for DFT/B3LYP and 0.9624 for DFT/ CAM-B3LYP to scale the frequencies [37]. The calculated vibrational frequencies and their corresponding assignments were investigated in detail by potential energy distribution (PED) analysis using VEDA 4 program [38]. The Chem Craft program [39] was used to evaluate the theoretical IR spectrum. Also the components of the electric moments such as total dipole moment (μ), mean polarizability $<\alpha>$ and total first hyperpolarizability (β) [40, 41] have been calculated and discussed at B3LYP and CAM-B3LYP functionals. Lastly in this study, the molecular docking of the title molecules and 6LU7 protein has been investigated by Swissdock online server.

2. Results and discussion

2.1. Geometry optimization

Alternate positions of enaminone group attached to 4-Hydroxy Benzo Hydrazide have been studied, but finally we get these three optimized structures of (E)-N′-((1H-Pyrrol-2-YL)Methylene) – 4-Hydroxy Benzo Hydrazide. Optimized parameters of 4-Hydroxy Benzo Hydrazide derivatives (three isomers of (E)-N′-((1H-Pyrrol-2-YL)Methylene) – 4-Hydroxy Benzo Hydrazide), calculated by B3LYP/CAM-B3LYP methods with 6–311 G (d, p) as the basis set are listed in supplementary Table 1, which are in accordance with the atom numbering scheme as shown in Fig. 1 also with the possible optimized structure of 4-Hydroxy Benzo Hydrazide. Local minimum energies are –778.7766 a.u., –778.7750 a.u., –778.7777 a.u. and –531.5123 for B3LYP while –778.3938 a.u., –778.3919, –778.3950, –531.3831 for CAM-B3LYP methods for I, II, III and 4HBH respectively given in Table 1. Optimized structures of 4-HBH, I, II and III have C1 point group symmetry. In I, II and III, Both rings are not in the same plane as the molecules are twisted from the middle chain. C–C bond distances are found to be in the range of 1.388–1.499 A°, 1.383–1.466 A° & 1.383–1.466 A° for B3LYP and 1.382–1.495 A°, 1.378–1.466 A° & 1.378–1.467 A° for CAM-B3LYP respectively for isomers I, II and III. For C–O, these values are 1.361 A°, 1.345–1.362 A° & 1.337–1.361 A° for B3LYP and 1.355 A°, 1.337–1.356 A° & 1.329–1.355 A° for CAM-B3LYP respectively. In case of C–H bond distances, they lie in the range of 1.083– 1.096 A°, 1.078–1.086 A° & 1.078–1.087 A° for B3LY P and 1.078– 1.085 A°, 1.078–1.090 A° & 1.078–1.087 A° for CAM-B3LYP, respectively. The C–C bond distance of literature compound [29] i.e. BH lies in the range 1.391–1.40A while the ring C–H bond distances were found 1.085A. The longer C–C bond distance in title compound shows that there is no delocalization of the nitrogen lone pair of electrons towards the ring. Planes of the benzene ring and the planar hydrazide group of 4-Hydroxy Benzo Hydrazide are inclined at 24.5° with respect to each other. Except amino and hydrazide hydrogens, molecule is essentially planar as evidenced by the torsion angles C6–C1–C7–O8, N10–N9–C7–C1 and N10–N9–C7–O8 of –23.3°, –23.2° and 158.5°. Here we have seen that calculated bond lengths by B3LYP method are very closer to literature [29]. This shows the supremacy of B3LYP method over CAM-B3LYP.

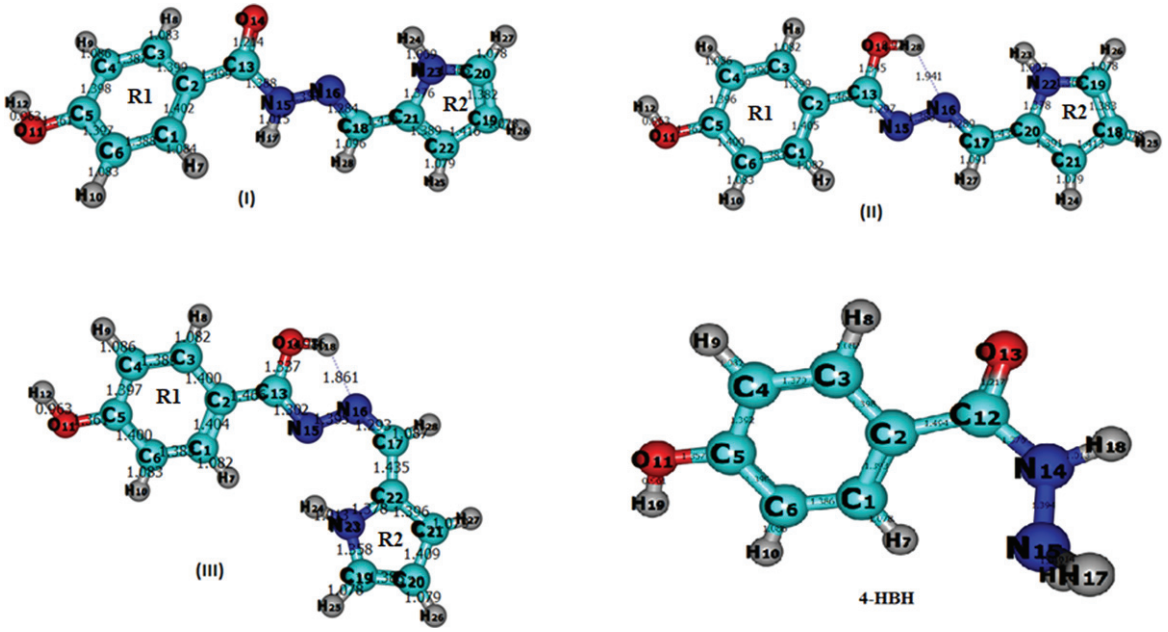

Fig. 1. Model Molecular Structure of 4-HBH and three isomers of title compound.

Table 1
Comparative energy (in a.u.) of 4HBH and the three Isomers of title compound at 6–311 G (d,p) level

Functional	Isomer 1	Isomer 2	Isomer 3	4HBH
B3LYP	–778.7766	–778.7750	–778.7777	–531.5123
CAM-B3LYP	–778.3938	–778.3919	–778.3950	–531.3831

2.2. *Vibrational analysis*

The 4-HBH contains 19 while its derivatives (I, II and III) have 28 atoms and they have 51 and 78 normal modes of vibration, respectively. All the fundamental vibrations are active IR. The harmonic vibrational frequencies are calculated at B3LYP/CAM-B3LYP and 6–311 G (d, p) level and experimental frequencies {FTIR and FTRaman- supplementary Fig. 1 (a & b)} have been recored for 4-Hydroxy Benzo Hydrazide only. No experimental FTIR spectrum for 4-Hydroxy Benzo Hydrazide derivatives is available for comparison so the theoretical spectrum (supplementary Figure 2) will be a suitable path for experimental researchers. Vibrational assignments of the normal modes of I, II and III are discussed in Table 2, 3 and 4. A comparison of all IR spectrum is shown in Fig. 2. Vibrational assignments are based on the observation of the animated modes in GaussView and discussed below.

2.3. *(O–H) and (C–H) vibrations*

The aromatic C–H stretching vibrations lie in the range 3100–3000 cm^{-1} [42]. The C–H stretching vibrations for 4-Hydroxy Benzo Hydrazide are observed at 3081(Raman) and 3012 (IR) cm^{-1} which are in good agreement with the aromatic C–H stretching frequencies, observed at 3062, 3047, 3060 and 3080 cm^{-1} of benzene and its derivatives [43]. The aromatic C–H present in the benzene ring of BH are seen as medium to strong bands in IR at 3062, 3050 and 3027 cm^{-1} [29]. In accordance with the bending vibrations of benzene [44] the peaks seen at 1090, 1049 cm^{-1} (IR) and 1046 cm^{-1} (Raman) in

Table 2
Comparison of the calculated Vibrational spectra with assignments of I by B3LYP/CAM-B3LYP/6-311 G (d, p) methods

B3LYP		CAM-B3LYP		Vibrational Assignment
Scaled Freq.	IR intensity	Scaled Freq.	IR intensity	
483	42.8554	477	51.6086	β_{out} (15N–17H) (43%)
490	23.387	497	13.6821	R1[β_{out} (C–C–C) + β_{out}(C–H)] + β_{out} (15N–17H) (21%)
526	22.3151	533	22.0461	R1[β_{out} (C–C–C) + β_{out}(C–H)]
549	48.2771	573	50.1374	β_{out} (23N–28H) (69%)
606	32.765	640	32.0031	Ring R1 Breathing
651	48.3251	689	51.2412	β_{out} (11O–12H) (24%)] + R1[τ (C–C–C–C) (21%)]
704	91.7578	722	94.6277	β_{out} (19C–26H) (36%) + β_{out} (20C–27H) (29%)
739	26.5499	756	32.411	R1[β_{out} (C–C–C) + β_{out}(C–H)] + β_{out}(13C–14O) (17%)
773	21.6174	799	16.4497	R2[β_{out} (C–C–C) (31%) + β_{out}(C–H) (18%)]
816	31.1816	835	32.7719	R1[β_{out} (C–C–C) (28%) + β_{out}(C–H) (32%)]
857	12.2726	877	10.6485	R2[β (C–C–C) (61%) + β (C–H) (21%)]
881	23.8969	895	29.036	Ring R1&R2 Breathing
908	11.2773	933	12.1061	β (18C–28H) (81%)
952	37.713	966	32.4391	R2[β(C–N–C) (15%) + β (C–C–C) (21%) + β(C–H) (31%)]
1012	52.1344	1016	54.2541	β (19C–26H) (26%) + β (22C–25H) (19%)
1037	12.3927	1060	10.0571	R2[β(C–N–C) + β (C–C–C) + β(C–H)]
1066	44.9576	1079	53.4016	R1[β (C–C) (24%) + β(C–H)](31%) + β(11O–12H) (14%)
1083	73.279	1092	51.5572	β (23N–24H) (21%) + β (20C–27H) (15%)
1094	39.0411	1104	24.8774	β (15N–17H) (13%) + υ(15N–116N) (17%) + R1[β (C–C) + β(C–H)] + β(11O–12H) (14%)
1123	190.888	1147	23.2847	R1 β (C–C) (39%) + β(C–H) (32%)] + β(11O–12H) (22%)
1142	302.9124	1152	460.2024	β(11O–12H) (27%)] + β (4C–9H) (15%)
1150	123.5665	1156	69.9927	υ (13C–2C) (25%) + β(15N–17H) (19%) + R1[β (C–C) + β(C–H)] + β(11O–12H) (12%)
1208	281.8507	1227	36.7442	R2[β(C–N–C) (17%)] + β (C–C–C) (24%) + β(C–H) (13%)] + β(18C–28H) (11%)
1216	82.5483	1238	350.4964	R1 β (C–C) (33%) + β(C–H) (21%)] + β(11O–12H) (12%)
1247	107.1672	1270	145.3033	R2[β(C–N–C) (29%)] + β (C–C–C) (37%) + β(C–H) (24%)] + β(18C–28H) (14%)
1261	24.8574	1273	25.0607	R2[β(C–N–C) + β (C–C–C) + β(C–H)]
1300	39.717	1315	70.9183	β (28H–18C) (29%) + β(15N–17H) (23%) + β(22C–25H) (17%)
1316	36.8194	1318	8.9768	R1[υ (C–C) (35%) + β(C–H) (32%) + β(11O–12H) (21%)
1395	17.8486	1419	26.3573	υ (23N–21C) (45%) + β(23N–24H) (32%)
1396	34.6263	1426	10.801	R2[β(C–N–C) (17%)] + β (C–C–C) (37%) + β(C–H) (34%)]
1405	20.4706	1429	31.4119	R1[υ (C–C) (25%) + β(C–H) (32%)] + β(11O–12H) (12%)
1423	10.0616	1449	17.464	υ (20N–22C) (27%)] + R2[υ (C–C) (32%) + β (C–H) (19%)] + β (15N–17C) (13%)
1475	345.1893	1497	449.4911	R1[υ (C–C) (23%) + β(C–H) (32%)] + β (15N–17C) (11%)
1492	119.7245	1568	107.6335	β (15N–17C) (15%) + β (18C–28H) (11%) + R1[υ (C–C) (23%) + β(C–H) (21%)]
1533	65.0114	1588	79.4396	R2[β (C–N–C) (29%)] + R2[υ(C–C) (37%)
1561	17.644	1599	13.4733	R1[υ (C–C) (33%) + β(C–H) (41%)] + β(11O–12H) (11%)

(*Continued*)

Table 2
(*Continued*)

B3LYP		CAM-B3LYP		Vibrational Assignment
Scaled Freq.	IR intensity	Scaled Freq.	IR intensity	
1587	127.5757	1625	155.7993	R1[υ (C–C) (36%) + β(C–H) (49%)]
1608	98.9418	1670	50.815	υ(16N–18C) (49%) + υ(21C–18C) (32%)
1693	278.3323	1741	288.0971	υ(14O–13C) (89%)
2916	45.9041	2948	41.8969	υ(28H–18C) (83%)
3026	23.5403	3051	17.7611	υ(9H–4C) (73%)
3041	11.8602	3065	10.3821	υ(7H–1C) (43%) + υ (10H–5C) (48%)
3372	7.5641	3423	9.2716	υ(15N–17H) (89%)
3497	70.3324	3519	84.7768	υ(23N–24H) (99%)
3674	91.5524	3716	103.5788	υ(11O–12H)[100%]

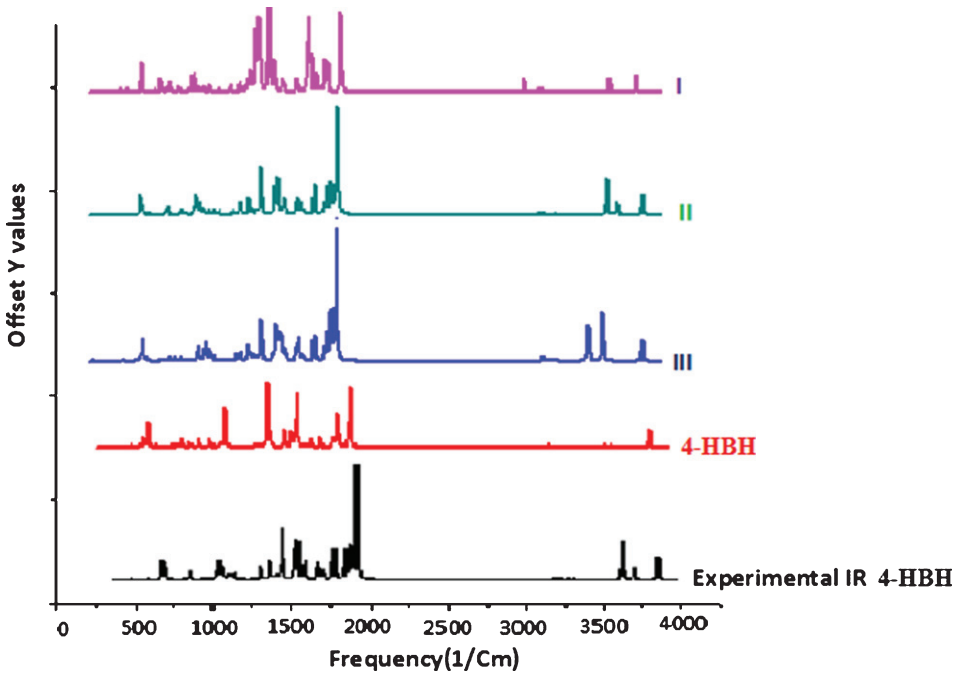

Fig. 2. Comparative IR spectra of all compounds.

4-Hydroxy Benzo Hydrazide spectra are attributed to the C–H in-plane bending vibrations. The ring C–H out of plane bending vibrations of 4-Hydroxy Benzo Hydrazide are seen in the infrared spectrum at 965, 956, 941 and 777 cm^{-1} [43]. The stretching frequency of O–H is identified at 3428 cm^{-1} in IR spectrum while it at 3430 cm^{-1} in calculated data. The O–H in-plane bending mode is identified at 1257 cm^{-1} in the IR and at 1255 cm^{-1} in Raman spectra whereas the out of plane bending mode is identified at 631 cm^{-1} in the IR and at 641 cm^{-1} in Raman spectra which are in good agreement with calculated data. Experimental frequencies nearly matches with the the calculated frequencies of B3LYP as campared to CAM-B3LYP method. In vibrational assignments, the C–H and O–H stretching vibrations are in the same range for all the derivatives (I, II, III) discussed in Table 2, 3 and 4.

Table 3
Comparison of the calculated Vibrational spectra with assignmentsof II by B3LYP/ CAM-B3LYP/6-311 G (d, p) methods

B3LYP		CAM-B3LYP		Vibrational Assignment
Scaled Frequency	IR intensity	Scaled Frequency	IR intensity	
350	118.4313	363	124.9219	β_{out} (11O–12H) (54%)
362	18.2986	382	17.439	R1[[τ(C–C–C–C) (11%) + τ (2C–13C–14O–28H) (17%)] + τ (15N–16N–17C–28H) (21%)
512	58.9415	555	57.4514	β_{out} (22N–23H) (46%)
612	24.4195	645	22.456	Ring R1 Breathing
643	7.477	681	10.6966	β_{out} (14O–28H) (26%)] + R1[τ (C–C–C–C) (31%)]
697	27.2591	740	40.1221	β_{out} (14O–28H) (24%)] + R1[τ (C–C–C–C) (21%)]
706	96.6931	754	91.9246	R2[β_{out} (C–H) (35%)]
732	78.2065	780	82.918	R1[[τ(C–C–C–C) (23%)] + [τ (2C–13C–14O–28H) (19%)
764	22.8306	806	25.7312	R2[β (C–H) (29%) + β (C–C) (31%)]
783	8.1018	841	14.281	β_{out} (21C–24H) (18%) + β_{out}t (18C–25H) (24%) + β_{out} (19C–26H) (42%)
797	19.4004	844	17.6158	R1[β(C–C–C) (38%)]
821	31.1122	873	32.7204	β_{out} (1C–7H) (28%) + β_{out} (5C–10H) (32%)
941	10.26	1004	11.8064	β(10C–26H) (35%) + β (18C–25H) (39%)
949	16.8708	1007	10.2561	β(17C–27H) (47%)
998	43.4569	1061	86.0462	β(21C–24H) (38%) + β (18C–25H) (42%)
1015	55.8184	1068	17.2139	β(21C–24H) (27%) + υ(15N–16N) (16%) + β(17C–27H) (22%)
1065	76.0312	1123	88.908	R2[β (C–H) (47%) + β (N–H) (29%)]
1075	31.006	1133	22.399	R1[β (C–H) (61%)]
1104	14.0347	1173	18.7888	R1[β(C–C) (27%) + β(C–H) (39%)] + υ(15N–16N) (17%)
1142	150.386	1198	26.7802	R1[β (C–H) (71%)]
1149	172.7663	1204	253.243	β(11O–12H) (89%)]
1233	129.7987	1299	135.9068	β(14O–28H) (77%)]
1246	162.2252	1322	176.7406	R1[β (C–C–C) (19%) + β(C–H) (22%)] + β(17C–27H) (11%) + R2[β(C–H) (23%)]
1258	28.083	1322	11.4024	R2[β (C–H) (23%)] + R2[β(N–H) (11%)] + β(17C–27H) (21%)
1278	16.0233	1339	10.6391	R1[β (C–C–C) (10%)] + R1[β(C–H) (21%)]
1292	26.6546	1365	57.2207	R1[β (17C–27H) (57%)] + R2[β(C–H) (17%)
1316	69.5266	1371	65.1115	R1[β (C–H) (37%)] + R1[β(C–C) (32%) + R2[β (11O–12H) (26%)]
1375	81.3562	1456	116.5657	υ (13C–14O) (29%) + β(14O–28H) (16%) + R1[β (C–H) (13%)
1390	24.9431	1484	13.6506	υ(20C–22N)[31%] + υ(19C–22N)[29%] + β (22N–28H)19%
1404	29.623	1485	44.6845	R2[β (C–C) (31%)] + R2[β(C–H) (27%) + υ(20C–22N)[15%]

(*Continued*)

Table 3
(*Continued*)

B3LYP		CAM-B3LYP		Vibrational Assignment
Scaled Frequency	IR intensity	Scaled Frequency	IR intensity	
1415	11.7508	1496	11.7704	R1[β (C–H) (21%)] + R1[β(C–C) (12%) + R2[β (N–H) (11%)] + R2[β(C–H) (17%)
1423	16.6892	1508	25.2429	R2[β (C–N–C) (39%)] + [υ(C–O) (31%)
1486	211.4073	1577	189.6982	R1[β (C–H) (35%)] + R1[υ(C–C) (43%) + υ (15C–13N) (17%)
1544	156.9155	1658	149.6037	R1[β (C–H) (43%)] + R1[υ(C–C) (37%) + β(13N–14O–28H) (16%) + υ (15C–13N) (13%)
1571	43.281	1694	147.1628	R1[β (C–H) (50%)] + R1[υ(C–C) (42%)
1589	131.7016	1696	97.5399	υ(17C–16N) (17%) + υ (15C–13N) (21%) + β(13N–14O–28H) (27%) + R1[υ(C–C) (32%)
1612	707.6691	1736	803.3336	υ(17C–16N) (37%) + υ (15C–13N) (26%) + β(13N–14O–28H) (29%)
2981	14.1793	3136	9.894	R1[υ(17C–27H) (24%)]
3026	28.8138	3177	22.1502	R1[υ(9H–4C) (41%) + υ (8H–3C) (58%)]
3425	143.2864	3622	186.5282	υ(14O–28H) (98%)
3522	47.8866	3695	58.2308	υ(22N–23H) (99%)
3673	103.6369	3870	112.2172	υ(11O–12H)[100%]

2.4. (C–C) and (N–H) vibrations

The aromatic ring carbon–carbon stretching modes of benzene and its derivatives are noticed in the range of 1650–1200 cm^{-1} [45, 46]. Strong to medium lines as observed in the IR spectrum of 4-HBH at 1591, 1539, 1512, 1467, 1340 and 1282 cm^{-1} are described to the C–C stretching modes. Strong bands in IR at 1607 cm^{-1} and at 1612 cm^{-1} in Raman are assigned to the –NH2 deformation mode of 4-Hydroxy Benzo Hydrazide while in literature, The aromatic ring carbon–carbon stretchingmodes are also expected in the range from 1650 to 1200 cm^{-1}. Benzene has two degenerate modes at 1596 cm^{-1} and 1485 cm^{-1}. Similarly the frequency of two non-degenerate modes observed at 1310 cm^{-1} and 995 cm^{-1} in benzene [43]. The N–H stretching vibration of hydrazide group appears at 3280 cm^{-1} in IR and at 3256 cm^{-1} in Raman spectra. The N–H stretching vibrations are normally viewed in the region 3300–3600 cm^{-1}. For isomer I, the N–H stretching vibration is calculated at 3372 cm^{-1} while it is 3522 and 3420 cm^{-1} for isomer II and III respectivelly. In lower region (below 800 cm^{-1}), torsional vibration of C=C–N–H are also seen in the assignment of all isomers (I, II & III). For isomer I, the C–C stretching vibrations are calculated at 1492 (1568) cm^{-1} while it is at 1486 (1577) and 1484 (1576) cm^{-1} [B3LYP(CAM-B3LYP)] for isomer II and III respectivelly.

2.5. Other modes of vibration

In 4-Hydroxy Benzo Hydrazide, the ring breathing mode is calculated at 602 cm^{-1} which is in good agreement with the experimental data, that is, 605 cm^{-1}, while in all the derivatives (I,II, III), ring breathing modes are at 606 (640), 612 (645), and 610 (642) cm^{-1} having appropriate IR intensity. As expected, torsion modes along with wagging modes appear in the lower frequency range. For 4-Hydroxy Benzo Hydrazide, strong torsion mode of C–C–C–C is at 564 cm^{-1} in calculated spectrum which matches well with the experimental one, that is, 570 cm^{-1},while strong torsion modes of C–C–C–C

Table 4
Comparison of the calculated Vibrational spectra with assignmentsof III by B3LYP/ CAM-B3LYP/6-311 G (d, p) methods

B3LYP		CAM-B3LYP		Vibrational Assignment
Scaled Frequency	IR intensity	Scaled Frequency	IR intensity	
367	108.2927	377	109.2724	β_{out} (11O–12H) (54%)
385	10.8785	407	11.7887	R1[[τ(C–C–C–C) (11%) + τ (2C–13C–14O–28H) (17%)] + τ(15N–16N–17C–28H) (21%)
531	22.4624	567	22.3186	β_{out} (22N–23H) (46%)
571	21.3294	602	19.5022	Ring R1&R2 Breathing
587	10.87	626	12.3398	R2[[τ(C–N–C–C) + τ (H–C–C–H)]
610	10.4678	642	10.523	Ring R1 Breathing
647	1.7592	688	1.6907	β_{out} (14O–28H) (26%)] + R1[τ (C–C–C–C) (31%)]
686	3.3197	730	5.3781	R2[β_{out} (C–H) (35%)]
717	37.3949	763	37.4237	R2[β_{out} (C–H) (35%)]
722	56.7497	769	60.1092	R1[[τ(C–C–C–C) (23%)] + [τ (2C–13C–14O–28H) (19%)
767	33.4405	809	34.1047	R2[β (C–H) (29%) + β (C–C) (31%)]
774	99.9665	821	123.2933	β_{out} (21C–24H) (18%) + β_{out} (18C–25H) (24%) + β_{out} (19C–26H) (42%)
791	56.0716	848	40.1394	R1[β(C–C–C) (38%)]
805	12.3208	852	15.9248	β(15N–16N–17C) (24%) + R2[β(C–N–C) + β(C–C–C) + β(C–H)]
816	24.8227	869	23.7864	β_{out} (1C–7H) (28%) + β_{out} (5C–10H) (32%)
851	0.0005	909	10.9717	R1[β(C–C–C) + β(C–H)] + R2[β(C–N–C) + β(C–C–C) + β(C–H)]
942	18.9666	1002	1.6787	β(10C–26H) (35%) + β(18C–25H) (39%)
965	28.5874	1036	32.1442	β(17C–27H) (47%)
985	0.9315	1040	12.0086	β(21C–24H) (38%) + β(18C–25H) (42%)
1017	47.1457	1064	49.7147	β(21C–24H) (27%) + υ(15N–16N) (16%) + β(17C–27H) (22%)
1059	87.0593	1117	100.0931	R2[β (C–H) (47%) + β (N–H) (29%)]
1079	35.875	1134	28.1347	R1[β (C–H) (61%)]
1096	37.8923	1153	25.7973	β(20C–26H) (37%) + β(21C–27H) (41%)
1103	5.7146	1171	21.5208	R1[β(C–C) (27%) + β(C–H) (39%)] + υ(15N–16N) (17%)
1143	133.6493	1199	22.9502	R1[β (C–H) (71%)]
1151	166.1405	1205	236.3207	β(11O–12H) (89%)]
1217	20.1759	1282	23.0342	β(14O–28H) (77%)]
1237	190.1962	1308	183.314	R1[β (C–C–C) (19%) + β(C–H) (22%)] + β(17C–27H) (11%) + R2[β(C–H) (23%)]
1249	142.0432	1325	144.2228	R2[β (C–H) (23%)] + R2[β(N–H) (11%)] + β(17C–27H) (21%)
1270	67.8627	1335	28.8497	R1[β (C–C–C) (10%)] + R1[β(C–H) (21%)]
1279	88.7216	1344	145.3576	R1[β (17C–27H) (57%)] + R2[β(C–H) (17%)
1314	34.5646	1370	56.246	R1[β (17C–27H) (57%)] + R2[β(C–H) (17%)

(*Continued*)

Table 4
(*Continued*)

B3LYP		CAM-B3LYP		Vibrational Assignment
Scaled Frequency	IR intensity	Scaled Frequency	IR intensity	
1318	32.6606	1388	29.7065	R1[β (C–H) (37%)] + R1[β(C–C) (32%) + R2[β (11O–12H) (26%)]
1374	66.1348	1455	85.4573	υ (13C–14O) (29%) + β(14O-28H) (16%) + R1[β (C–H) (13%)
1383	55.1456	1467	108.9683	υ(20C–22N)[31%] + υ(19C–22N)[29%] + β (22N–28H)19%
1388	34.3131	1480	3.8144	R2[β (C–C) (31%)] + R2[β(C–H) (27%) s+ υ(20C–22N)[15%]
1415	10.8257	1496	20.0693	R1[β (C–H) (21%)] + R1[β(C–C) (12%) + R2[β (N–H) (11%)] + R2[β(C–H) (17%)
1428	8.8952	1513	10.8952	R2[β (C–N–C) (39%)] + υ(C–O) (31%)
1484	201.5601	1576	185.4923	R1[β (C–H) (35%)] + R1[υ(C–C) (43%) + υ (15C–13N) (17%)
1545	186.5887	1657	167.0252	R1[β (C–H) (43%)] + R1[υ(C–C) (37%) + β(13N–14O–28H) (16%) + υ (15C–13N) (13%)
1574	42.6826	1694	120.2316	R1[β (C–H) (50%)] + R1[υ(C–C) (42%)
1589	117.7402	1696	251.6079	υ(17C–16N) (17%) + υ (15C–13N) (21%) + β(13N–14O–28H) (27%) + R1[υ(C–C) (32%)
1605	723.5927	1730	696.6936	υ(17C–16N) (37%) + υ (15C–13N) (26%) + β(13N–14O–28H) (29%)
3020	12.2277	3171	10.2649	R1[υ(17C–27H) (24%)]
3027	25.2308	3179	19.3602	R1[υ(9H–4C) (41%) + υ (8H–3C) (58%)]
3298	189.0629	3492	220.0088	υ(14O–28H) (98%)
3420	222.3406	3592	271.9228	υ(22N–23H) (99%)
3674	103.9801	3870	114.1538	υ(11O–12H)[100%]

are at 651, 697 and 647 cm^{-1} in calculated spectrum for isomer I, II and III respectively. A very strong stretching vibration of C=O is found at 1693 (1741) cm^{-1} for isomer I while C–O vibrations are at 1423 cm^{-1} and 1430 cm^{-1} in calculated spectra for isomer II and III. In literature [29], the frequency of the carbonyl stretching vibration is absorbed at 1661 cm^{-1} in the infrared spectrum, the reason being that the double bond character of the C=O group is less due to the nitrogen lone pair electron being delocalized towards the carbonyl end. There are some frequencies in lower region having appreciable IR intensity. Furthermore, the study of low frequency vibrations is of great significance, because it gives information on weak intermolecular interactions, which take place in enzyme reactions [47]. Knowledge of low frequency mode is also essential for the interpretation of the effect of electromagnetic radiation on biological systems [48]. The full interpretation of vibrational spectra of 4-Hydroxy Benzo Hydrazide and its derivatives is in good agreement with the literature [49]. The aim of vibrational analysis is to acquire direct information on lower and higher frequency vibrations of such 4-Hydroxy Benzo Hydrazide and its derivatives. No experimental FTIR spectrum is available for comparison for derivatives of 4-Hydroxy Benzo Hydrazide so it will provide a suitable path for experimental researchers.

2.6. Electronic properties and TDDFT analysis

Frontier orbital energy gap, that is, the gap between HOMO and LUMO, shows the interaction of that molecule with other species. Frontier orbital energy gap helps to differentiate the chemical reactivity of the molecules [50, 51]. In case of 4-Hydroxy Benzo Hydrazide and its derivatives (I, II nad III), frontier orbital energy gap is 5.35792, 2.03075, 3.62059 and 3.79059 eV, respectively for B3LYP method, and is given in Table 5 with CAM-B3LYP method too. In literature [29], the frontier orbital energy gap of benzo hydrazide is nearly 5.6052 eV, So it can be concluded that isomer I is the most reactive compound among all. The HOMOs and LUMOs are seen to be localized on molecules as a whole for 4-Hydroxy Benzo Hydrazide, isomers II and III while for isomer I, the LUMOs are seen to be localized on molecules as a whole but HOMOs are seen over enaminone group only. Molecular electrostatic potential maps are very useful three dimensional diagrams of molecules. They enable us to visualize the charge distributions of molecules and charge related properties of molecules. They also allow us to visualize the size and shape of molecules. In organic chemistry, electrostatic potential maps are invaluable in predicting the behaviour of complex molecules [52]. The pictures of HOMO, LUMO and electrostatic potential (MESP) for 4-HBH and derivatives (I, II & III) are shown in Fig. 3 & 4 respectivelly. DOS plot (Supplementary Figure 3) shows the features of the Molecular Orbital in a specific energy selection and population analysis per orbital. It shows interaction of anti-bonding or bonding characters among two orbitals. The edge is calculated by the degree of negative (anti-bonding interaction) and positive (bonding interaction) overlap for a specific MO. It illustrates anti-bonding charm of both the frontier orbitals. Charge localization over HOMO, LUMO as well as for affiliated MO are verified with the plot.

TDDFT method is an important tool for studying the nature of the transitions and UV spectrum of the title compound. TDDFT of title molecules are calculated by using combination of DFT/B3LYP and 6–311G(d, p) as the basis set. The calculated high oscillatory strength of electronic transitions are listed in Table 6 and shown in supplementary Figure 4. A prominent peak occurs at 236 nm, 323 nm, 330 nm and 335 nm in 4-Hydroxy Benzo Hydrazide (4HBH) and its newly designed derivatve I, II, III respectively. In 4HBH prominent peaks occurs due to transition of electron from HOMO-1$\longrightarrow$LUMO, HOMO$\longrightarrow$LUMO, HOMO-2$\longrightarrow$LUMO, HOMO-2$\longrightarrow$LUMO + 1, HOMO-1$\longrightarrow$LUMO + 1 with 11%, 62%, 5% 3% and 4% contribution respectively. In I, II & III isomers, prominent peaks occurs

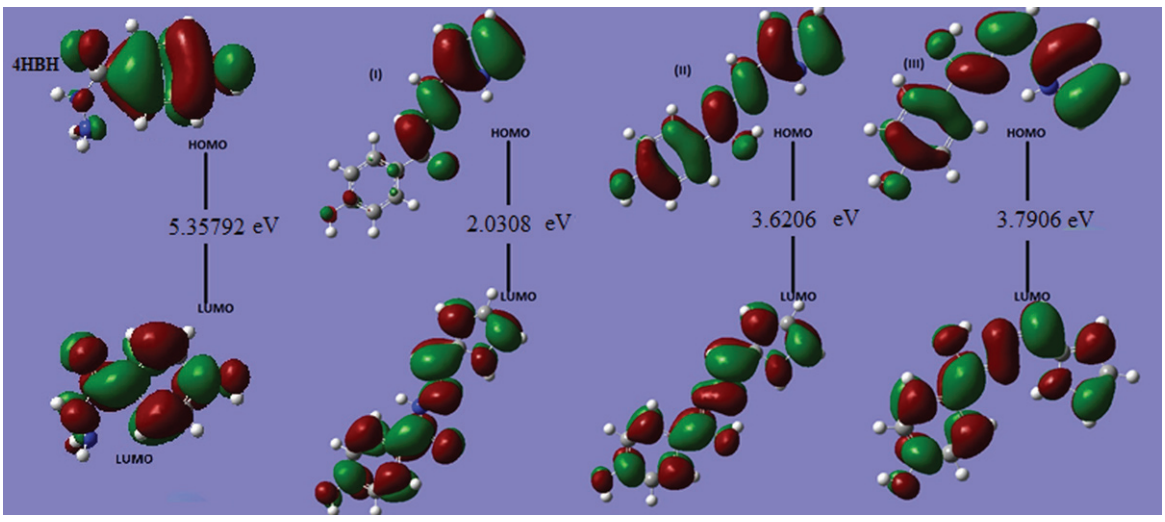

Fig. 3. LUMO-HOMO orbital Plots of 4-HBH and three isomers of title compound.

Table 5
HOMO-LUMO orbital energies (eV) and their energy band gap, dipole moment (D) of the three Isomers of title compound computed at B3LYP and CAM-B3LYP/6-311 G (d, p) level

Parameters	B3LYP				CAM-B3LYP			
	4HBH	Isomer I	Isomer II	Isomer III	4HBH	Isomer I	Isomer II	Isomer III
E_{LUMO}	–0.04106	–0.09246	–0.05607	–0.06032	–0.00399	–0.00762	–0.01428	–0.01794
E_{HOMO}	–0.23877	–0.16712	–0.18918	–0.19968	–0.27888	–0.25269	–0.23629	–0.24845
E_{GAP}	0.19771	0.07466	0.13311	0.13936	0.27489	0.24607	0.22201	0.23051
E_{GAP} (eV)	5.35792	2.03075	3.62059	3.79059	7.44952	6.66590	6.01647	6.24682
Dipole moment (μ)	5.02854	2.6453	2.2634	2.1035	5.0889	2.8119	2.2895	2.1053

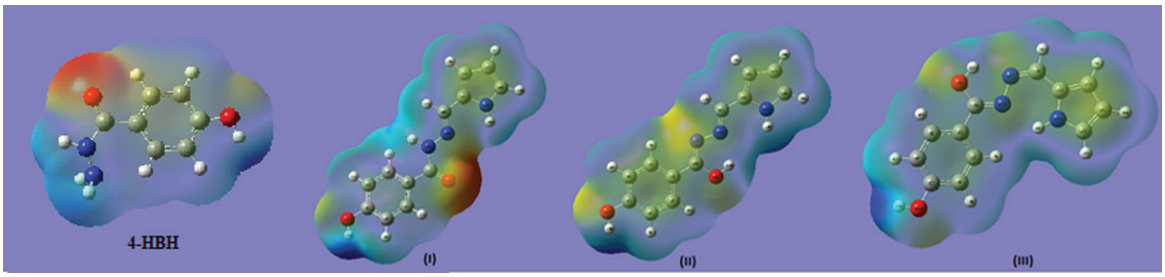

Fig. 4. MESP surfaces of 4-HBH and three isomers of title compound.

due to electronic transitions occurs from HOMO⟶LUMO with contribution 96% 100% 99% respectively. In I and III isomer, a bumf occurs at 286nm and 279 with their corresponding transition from HOMO⟶LUMO + 1(93%), HOMO⟶LUMO + 2(4%) and HOMO⟶LUMO + 1(91%), HOMO-4⟶LUMO (5%) respectively. On basis of assignment, these transition originated due to $\mathbf{n}_p \longrightarrow R_{y^*}$.

2.7. Optical, dipole moment and thermo-dynamical

Dipole moment (μ), polarizability <α> and total first static hyperpolarizability β [53, 54] can be expressed in terms of *x*, *y*, *z* components and are given by following equations 1, 2 and 3-

$$\mu = \left(\mu_x^2 + \mu_y^2 + \mu_z^2\right)^{1/2} \tag{1}$$

$$< \alpha > = 1/3 \left[\alpha_{xx} + \alpha_{yy} + \alpha_{zz}\right] \tag{2}$$

$$\beta_{Total} = \left(\beta_{x^2} + \beta_{y^2} + \beta_{z^2}\right)^{1/2}$$
$$= \left[\left(\beta_{xxx} + \beta_{xyy} + \beta_{xzz}\right)^2 + \left(\beta_{yyy} + \beta_{yxx} + \beta_{yzz}\right)^2 + \left(\beta_{zzz} + \beta_{zxx} + \beta_{zyy}\right)^2\right]^{1/2} \tag{3}$$

The β components of Gaussian output are reported in atomic units (where 1 a.u. = $8.3693^{*}10^{-33}$ e.s.u.). The calculated dipole moments (Table 5) for 4-Hydroxy Benzo Hydrazide and its derivatives are 5.02854, 2.6453, 2.2634 and 2.1035 Debye respectively. So, 4-HBH is a better solvent among them all. A greater contribution of α_{zz} (lesser of α_{xx}) is seen in all compounds that means these compounds are elongated more towards Z direction and is more contracted in the X direction. βxxx, βxxy and βyyy contribute lager part of hyperpolarizability in all the molecules. This shows that X-axis, XY plane and Y axis are more optically active in these directions. The values of hyperpolarizability

Table 6
The calculated electronic transitions: E (eV), oscillatory strength (f),λ_{max} (nm) using TD–DFT/B3LYP/6–311G (d, p)

S.N.	Electronic Transitions	E (eV)	Oscillatory Strength (f)	Calculated (λ_{max})	% Contribution	Assignment
			Isomer I			
1	H⟶L	3.84	0.723	323	96	$n_p \longrightarrow Ry^*$
2	H⟶L + 1	4.33	0.040	286	93	$n_p \longrightarrow Ry^*$
	H⟶L + 2				4	
3	H-3⟶L	4.43	0.037	280	59	$n_p \longrightarrow Ry^*$
	H-1⟶L				31	
	H-3⟶L + 2				2	
			Isomer II			
1	H⟶L	3.76	1.219	330	100	$n_p \longrightarrow Ry^*$
2	H-2⟶L	4.07	0.001	305	99	$n_p \longrightarrow Ry^*$
3	H-1⟶L	4.54	0.011	273	38	$n_p \longrightarrow Ry^*$
	H⟶L + 1				52	
	H-4⟶L				2	
	H⟶L + 2				3	
			Isomer III			
1	H⟶L	–	0.6475	335	99	$n_p \longrightarrow Ry^*$
2	H-2⟶L	–	0.0014	306	92	$n_p \longrightarrow Ry^*$
	H-1⟶L				5	
3	H⟶L + 1	–	0.0393	279	91	$n_p \longrightarrow Ry^*$
	H-4⟶L				5	
			4-Hydroxy-Benzo-Hydrazide			
1	H-2⟶L	4.83	0.0161	257	17	$n_p \longrightarrow Ry^*$
	H-1⟶L				56	
	H⟶L				13	
	H-3⟶L				5	
2	H-2⟶L	5.07	0.0114	245	30	$n_p \longrightarrow Ry^*$
	H⟶L + 1				56	
	H-3⟶L				6	
	H-1⟶L				6	
3	H-1⟶L	5.25	0.2595	236	11	$n_p \longrightarrow Ry^*$
	H⟶L				62	
	H-2⟶L				5	
	H-2⟶L + 1				3	
	H-1⟶L + 1				4	

indicate a possible use of these compounds in electro-optical applications. Supplementary Table 2 shows the values of polarizability and hyperpolarizability of 4-Hydroxy Benzo Hydrazide and its derivatives. Internal thermal energy (E), constant volume heat capacity C_v, and entropy S, calculated at B3LYP/CAM-B3LYP/6-311G (d, p) level, are listed in supplementary Table 3. We know that the conduction band is almost empty at the room temperature, so electronic contribution in total energy is negligible. Thermodynamic properties show that the vibrational motion plays an important role as compared to other motions.

2.8. NBO analysis

Natural bond analysis is an important tool for studying intermolecular and intramolecular interaction and charge transfer and conjugate interaction in molecular system [55]. The strength of interaction depend on second order perturbation energy $E^{(2)}$. The larger value of $E^{(2)}$ mean stronger interaction however lower $E^{(2)}$ value means weak interaction. The strength of delocalization interaction or second order energy For acceptor NBO (*j*) and, donor NBO (*i*), is related with second order energy lowering equation 4 as [56, 57]

$$E^{(2)} = -qi\frac{(F_{ij})^2}{\varepsilon_j - \varepsilon_i} \tag{4}$$

Here, q_i is the population of donor orbital or donor orbital occupancy, ε_i, ε_j are orbital energies (diagonal elements) of acceptor and donor NBO orbital's respectively, *Fij* is the off–diagonal Fock or Kohn–Sham matrix element between *i* and *j* NBO orbitals. NBO analyses of all compounds are calculated by using same level of theory are given in supplementary Tables 4, 5, 6 and 7.

In NBO analysis of 4-Hydroxy Benzo Hydrazide and its derivatives, significant interactions formed by orbital overlap between Lp(1)N/Lp(1)O, σ(N–N), π(C–C) and π^*(C–C), σ^* (C–C)/π^*(C–N) which stabilizes the system by inter molecular charge transfer. In 4-HBH, significant contribution occurs in between Lp(1)N14$\longrightarrow$ π^*(C12-O13), Lp(2)O13$\longrightarrow$ σ^*(C12–N13)/σ^*(C12–C2), Lp(2)O11$\longrightarrow$ π^*(C5–C6), π(C1–C2)$\longrightarrow$ π^*(C3–C4)/π^*(C5–C6)/π^*(C12–O13), which stabilize the molecule by 38 kcalmol^{-1}, 23 kcalmol^{-1}/18 kcalmol^{-1}, 30 kcalmol^{-1} 23 kcalmol^{-1}/16 kcalmol^{-1}/17 kcalmol^{-1} respectively. In isomer I of 4-HBH, most significant contribution occurs in between π(C1–C6) $\longrightarrow$ π^* (C3–C4)/ π^*(C5–C4), π(*C4–C5*) $\longrightarrow$ π^*(C1–C6)/ π^*(C2–C3), which stabilizes the molecules II and III by 17 kcalmol^{-1}/24 kcalmol^{-1}, 15 kcalmol^{-1}/24 kcalmol^{-1} and 17 kcalmol^{-1}/24 kcal mol^{-1},15 kcalmol^{-1}/23 kcalmol^{-1} respectively. In isomer II, two significant contribution came from lp(1)N15$\longrightarrow$ π^*(C13–N15), lp(1)O11$\longrightarrow$ π^*(C4–C5) which stabilizes isomer II by 44 kcalmol^{-1}, 30 kcalmol^{-1} respectively however in isomer III, two significant interaction occurs due to lp(1)N14$\longrightarrow$ π^*(C13–N15), lp(2)O11$\longrightarrow$ π^*(C4–C5) which stabilizes isomer III by 48 and 30 kcalmol^{-1} respectively. In isomer I, another significant contribution occurs due to orbital interaction between π(C1–C6) $\longrightarrow$ π^*(C2–C3)/ π^*(C4–C5), π(C4–C5) $\longrightarrow$ π^*(C1–C6)/ π^*(C2–C3), lp(1)N15$\longrightarrow$ π^*(C13–N15), lp(1)O11$\longrightarrow$ π^*(C4–C5) which stabilizes by 17 kcalmol^{-1}/25 kcalmol^{-1}, 16 kcalmol^{-1}/25 kcalmol^{-1}, 44 kcalmol^{-1}, 30 kcalmol^{-1} respectively. NBO analysis shows that most significant interaction occurs due to moment of π– electron cloud from donor to accepter which develops polarity of these isomers. The moment of π–electron clouds are responsible for the NLO activity these isomers.

Table 7

Calculated ε_{HOMO}, ε_{LUMO}, energy band gap ($\varepsilon_{LUMO} - \varepsilon_{HOMO}$), chemical potential ($\mu$), electronegativity ($\chi$), global hardness ($\eta$), global softness (S), and global electrophilicity index (ω) forI, II and III at B3LYP/6-311 G (d, p) level

Folder	ε_H	ε_L	ε_H - ε_L	χ	μ	η	S	ω
I	–0.16712	–0.09246	–0.07466	0.12979	–0.12979	0.03733	13.39405	3.47682
II	–0.18918	–0.05607	–0.13311	0.12262	–0.12262	0.06655	7.51258	1.84238
III	–0.19968	–0.06032	–0.13936	0.13000	–0.13000	0.06968	7.17566	1.86567
4HBH	–0.23877	–0.04106	–0.19771	0.13991	–0.13991	0.09885	5.05791	1.41530

2.9. Global reactivity descriptors

Global reactivity descriptors are described as –

$$\text{Energy band gap} = (\varepsilon_{\text{LUMO}} - \varepsilon_{\text{HOMO}}),$$

$$\text{Electronegativity } (\chi) = -1/2\ (\varepsilon_{\text{LUMO}} + \varepsilon_{\text{HOMO}}),$$

$$\text{Chemical potential } \mu = -\chi,$$

$$\text{Global hardness } \eta = 1/2\ (\varepsilon_{\text{LUMO}} - \varepsilon_{\text{HOMO}}),$$

$$\text{Global softness } (S = 1/2\eta)$$

$$\text{Global electrophilicity index } \omega = \mu 2/2\eta \qquad [58-62]$$

All these parameters for all compounds have been listed in Table 7.

According to these parameters, the chemical reactivity varies with the structural configuration of molecules. Chemical hardness (softness) value of compound (I) is lesser (greater) among all the molecules. Thus, compound (I) is found to be more reactive than all whereas, compound 4-HBH is less reactive. Compound 4-HBH possesses higher electronegativity (lower electrophilicity index) among them all. Correlations have been found between electrophilicity of various chemical compounds and reaction rates in biochemical systems.

2.10. Molecular docking

Hydrazides are well known pharmaceutical compound and show better activity against for anti-bacterial, antifungal, anticonvulsant activities In this segment, we calculate the biolocal activities of 4-HBH and its isomers (I, II, III). For this we first calculate their electro-topological indices like LogP,LogS by using ALOGPS 2.1 software [63]. This Program was developed by Tetko et.al. [64–66]. The calculated value of LogP is largest for isomer I however 4HBH have lowest Log *P* value. This means transportation through cell membranes varies according to I > III > II > 4-HBH. The value of Log S for 4HBH and its derivatives lies in between –2.78 to –1.33 however 85% drugs having Log S value lie in between –1 to –5.36. The calculated values of Log S are favouring the permeability for 4HBH and its isomers into cell are better through membranes. Several Biological activities of 4HBH and its derivatives are calculated by PASS software. By using molecular mechanics PASS predict 900 pharmacological effects e.g. mutagenicity, teratogenicity and embryo toxicity. The Biological activities are calculated by PASS more than 46,000 drugs whose biological activities are determined experimentally are selected as training set and 85% results predicted by PASS software are correct [67]. In Table-8, we have compared calculated biological activities of 4-HBH and its isomers. All (4HBH and its isomers) show good biological activity against Anti-tuberculosis and Antivirals. Now a day, COVID 19 is a serious disaster however a number of studies are being carried out on antiviral

Table 8
Biological activity of 4HBH and its Isomers predicted by PASS program

Biological Activity	I		II		III		4HBH	
	Pa	Pi	Pa	Pi	Pa	Pi	Pa	Pi
Antituberculosic	0.659	0.005	0.704	0.009	0.753	0.003	0.768	0.003
Antiviral	0.445	0.024	0.505	0.019	0.519	0.041	0.526	0.040

Table 9
Electrotopological indices like log Pand log S of I, II, III and 4HBH compounds

Parameter	I	II	III	4HBH
LogP	2.37	0.40	1.14	0.12
LogS	–2.78	–2.08	–2.65	–1.33
FF(a.u)	–1176.25	–1189.49	–1183.29	–1170.09
ΔG(kcal/mol)	–6.21	–6.58	–6.51	–6.37
Binding length(A^0)	1.978 A^0	2.147 A^0	3.310 A^0	2.061 A^0, 2.172 A^0
Binding Residue	**N119**	**GLN69**	**GLN69**	**MET17, GLU14**

and Anti-tuberculosis drugs to kill COVID 19 virus. In this way, our study has ability to become good drug for COVID19. To design new COVID 19 drug, first priority is to identify targets which, when inhibited, can kill the effected cells. In February 2020 researchers have identified COVID 19 protease and named as 6LU7. We have performed docking by using Swissdock online server [68] by using PDB file of 6LU7 protease [69]. Docking of 6LU7 protease with 4HBH and its isomers are blindly followed over whole molecules. The binding strength are describe by full fitness score (FF) and binding affinity. The more appropriate binding site between a ligand and its receptor is shown by highest negative FF score. The calculated FF, binding affinity, binding distance and binding site are listed in Table 9. The binding affinities (ΔG) obtained from docking of 6LU7 with I, II, III and 4HBH are – 6.21 kcal/mol, – 6.58 kcal/mol, – 6.51 kcal/mol and – 6.37 kcal/mol, respectively. The isomer-I, binds with polar Asparagine (N119) residue by distance 1.978 A^0 however isomers II and III bind with polar amino acid Glutamine (GLN69) residue with distances 2.147 A^0 and 3.310 A^0 respectively. The 4HBH binds with two residues amphipathic amino acid Methionine (MET17), and polar amino acid Glutamine (GLU14) with distance 2.061 A^0 and 2.172 A^0 respectively. Docking picture of I, II, III & 4HBH with 6LU7 protease are shown in Fig. 5. This study only provides a path to experimental researchers to designed new COVID 19 drug. This study is only based on molecular modelling and docking, not on clinical trials, as we did not consider its side effects and toxicity.

2.11. AIM analysis

At bond critical point (BCP) for any molecular system QTAIM [70], is important method to analyze the H–bonding and other interactions in terms of topological parameters. For nonbonding interactions [71] the electron density ($\rho_{\mathrm{H\,...\,A}}$) should lies within 0.002–0.040 a.u. ranges and Laplacian ($\nabla^2\rho_{\mathrm{BCP}}$) should varries in between 0.024–0.139 a.u. Based on this criteria, no H-bonding appears in isomer I however one H-bonding appears in 4HBH (N_{15}-H_7), isomer II (N_{16}-H_{28}) and two in isomer III (N_{15}-H_{24}, N_{16}-H_{18}).The AIM pictures of these compounds with BCP point(green color) are plotted in Fig. 6. The calculated topological parameters corresponding H-bonding intreactions for 4HBH and its derivatives e.g. electron density, $\rho(r)$, Laplacian $\Delta^2_{\rho(r)}$, $V(r)$, G(r),$H(r)$,ratio of V(r)/G(r) are listed in Table 10.

In energetically stable molecular system, the Laplacian $\Delta^2_{\rho(r)}$ [72] shows chemical characteristics of the system. This $\Delta^2_{\rho(r)}$ mainly shows connection in between charge density with bond length at BCP. In the case of 'closed shell' (hydrogen bonding (HB), van der Waals) interaction, Laplacian of the electron density $\Delta^2_{\rho(r)} > 0$. For closed shell interaction, $\rho_{(r)}$ is typically small (order of 10^{-2} au for HB and van der Waals interaction $10^{-2} - 10^{-3}$ au) which shows all interactions correspond to hydrogen bonding for all derivatives of benzo at BCP. The calculated value of $\rho_{(r)}$ lies within the range 0.0176–0.0397 a.u. however value of $\Delta^2_{\rho(r)}$ lies within the range 0.0657–0.1254a.u. The $\Delta^2_{\rho(r)} = 0.1254$ a.u. is strongest closed shell interaction among all other closed shell interactions. The sign and magnitude of the total

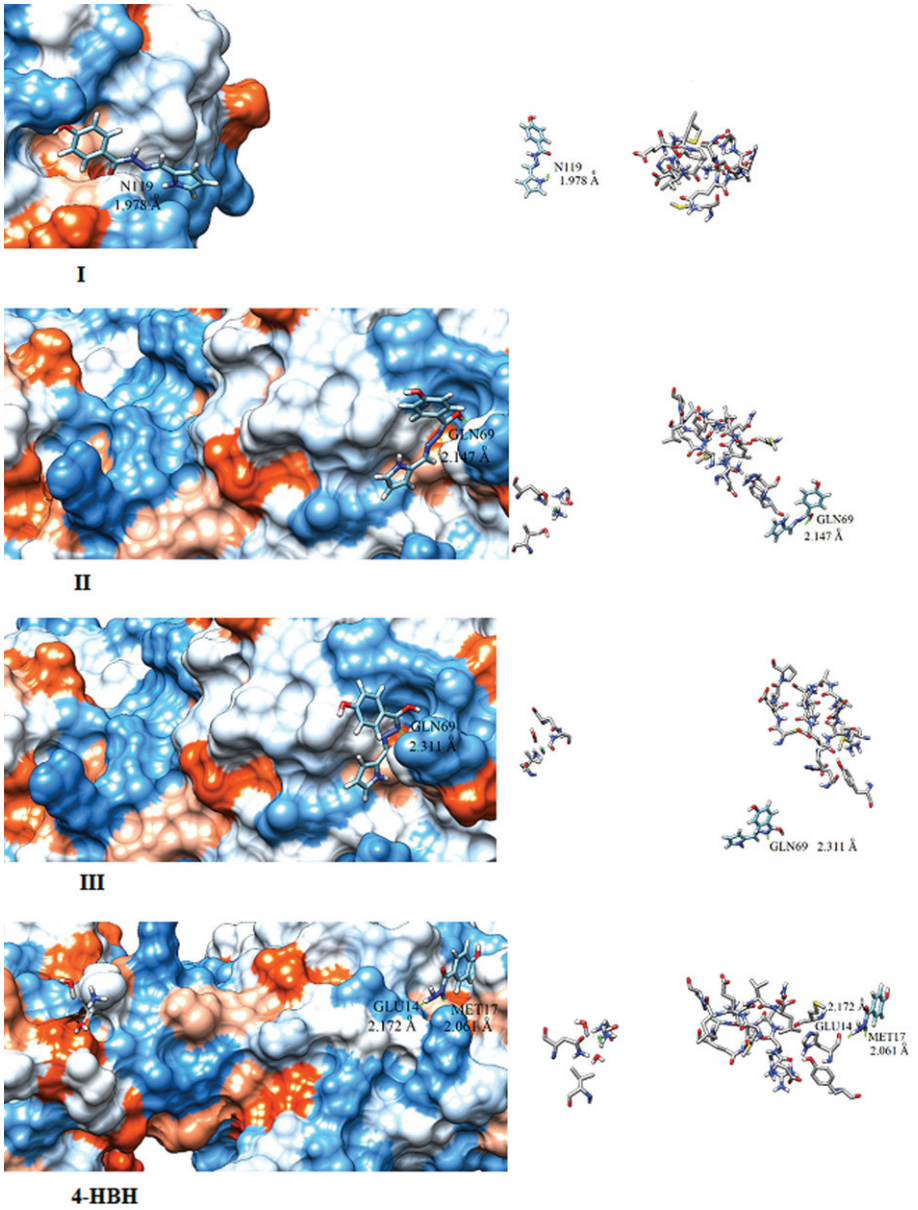

Fig. 5. Docking pictures of 4-HBH and I, II and III compounds.

energy densities [73] at a BCP $H(r) = G(r) + V(r)$, are also a useful indicator of the nature of bonding. The value of $V(r)$ is always negative however value of $G(r)$ is always positive. For II ($N_{16} - H_{28}$) and III ($N_{16} - H_{18}$), V(r) > G(r) shows H(r) < 0 which shows covalent bonding i.e. significant sharing of electrons dominates the interaction however in 4HBH, ($N_{15} - H_7$) $V(r) < G(r)$ or $H(r) > 0$ shows closed shell interactions (CSI) [74–76]. The useful information about nature of chemical bonding is given by $\left|\frac{V(r)}{G(r)}\right|$ parameter [77]. 4HBH (N15–H7), III (N15–H24) derivatives $\left|\frac{V(r)}{G(r)}\right| < 1$ corresponding H-bonding is ionic and Vander wall interactions however for II ($N_{16} - H_{28}$) and III ($N_{16} - H_{18}$) derivatives corresponding ratio is nearly equivalent to one hence partially covalent in nature. The $\sum_{i=1}^{3} \lambda 1, \lambda 2, \lambda 3$ are the principal curvatures of a bond attached BCP in Laplacian $\Delta^2_{\rho(r)}$. The ratio $\left|\frac{\lambda_1}{\lambda_2}\right|$ gives type of

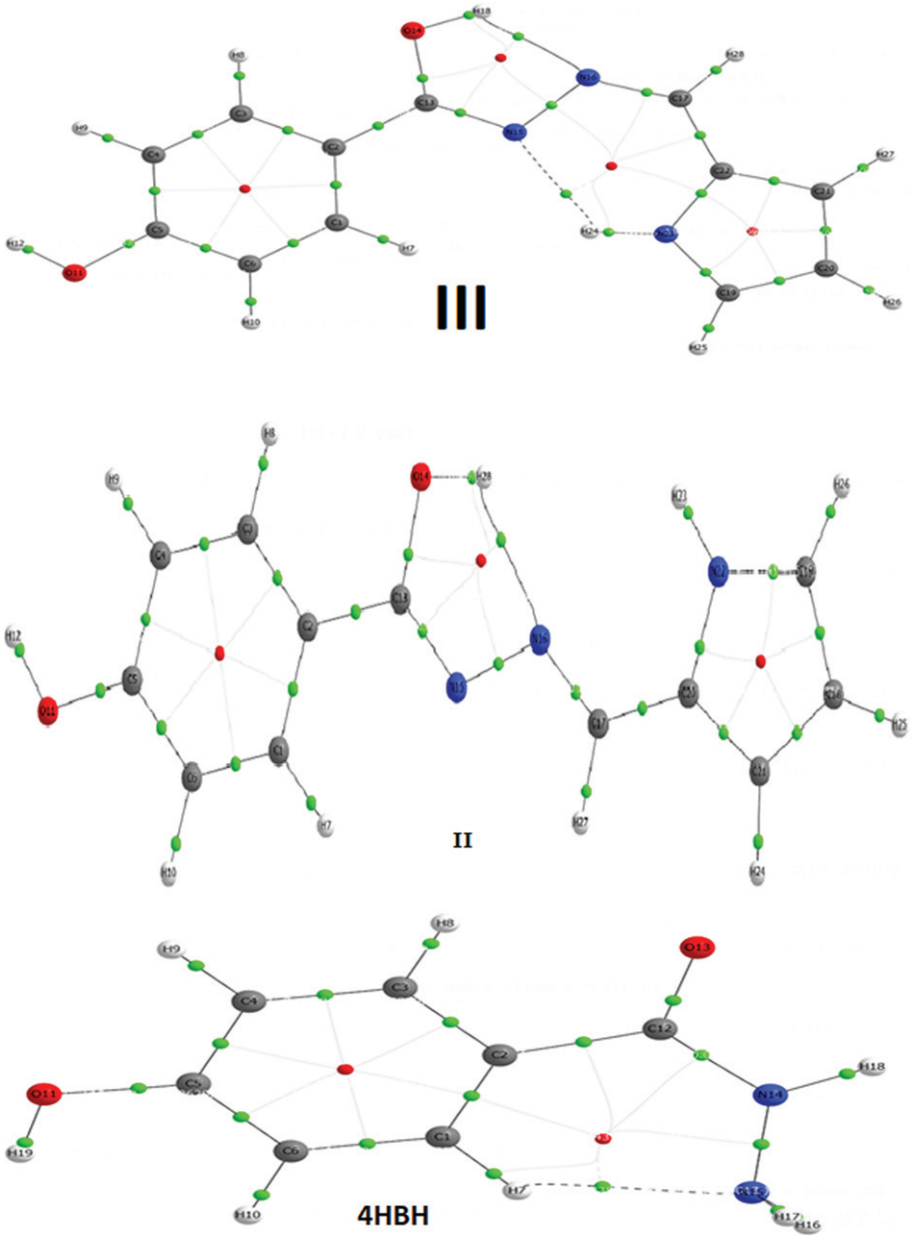

Fig. 6. AIM picture of III, II and 4HBH (Green dots represent BCP, Red dots represent ring critical).

interactions [78, 79]. In our study for all three derivatives $\left|\frac{\lambda_1}{\lambda_2}\right| < 1$ gives closed shell type intreaction which also classified a by $\nabla^2\rho_{bcp}$ criterion. The calculated value of $\left|\frac{\lambda_1}{\lambda_3}\right|$ for all bonds are listed in Table 10. The calculated value of $\left|\frac{\lambda_1}{\lambda_3}\right|$ are lies in between 0.196–0.240 which indicates all H-bonding are shows weak CSI bonding. The nature of H-bonding is also described by Rozas et al. [80] criteria. According to this criteria, in II ($N_{16} - H_{28}$) and III ($N_{16} - H_{18}$) derivatives $\nabla^2\rho > 0$ and $H < 0$ shows partially covalent nature however for 4HBH ($N_{15} - H_7$) and III (N_{15}-H_{24}), $\nabla^2\rho > 0$ and $H > 0$ shows that ionic nature which describe above by $\left|\frac{\lambda_1}{\lambda_3}\right|$ *paramereter* The strength of Hydrogen bonding in

Table 10
Topological parameters for bonds of interacting atoms: electron density (ρBCP), Laplacian of electron density (∇^2BCP), kinetic electron energy density (G BCP), potential electron energy density (VBCP), total electron energy density (HBCP), estimated interaction energy (E_{int}) at bond critical point (BCP)

Species	Bond	ρ_{bcp}	$\nabla^2\rho_{bcp}$	*Eigen value* $\nabla^2\rho_{bcp}$				G_{BCP}	V_{BCP}	$\left\lvert\frac{V(r)}{G(r)}\right\rvert$	H_{BCP}	E_{int} (kcal/mol)
				λ_1	λ_2	λ_3	$\left\lvert\frac{\lambda_1}{\lambda_3}\right\rvert$					
Benzo	N_{15}–H_7	0.0176	0.0657	–0.0318	–0.2198	0.1620	0.196	0.0151	–0.0140	0.927	0.0013	4.379
Benzo-1	–	–	–	–	–	–	–	–	–	–	–	–
Benzo-2	N_{16}–H_{28}	0.0333	0.1174	–0.0464	–0.3213	0.1958	0.237	0.0319	–0.0345	1.082	–0.0026	10.818
Benzo-3	N_{15}–H_{24}	0.0249	0.0884	–0.0289	–0.0278	0.1451	0.199	0.0199	–0.0178	0.894	0.0022	5.572
	N_{16}–H_{18}	0.0397	0.1254	–0.0551	–0.0492	0.2298	0.240	0.0337	–0.0361	1.071	–0.0024	11.326

terms of potential energy at BCP [81] given by relation $(\Delta E) = -\frac{1}{2V}$. According to this relation, bond energy for 4HBH ($N_{15} - H_7$) II ($N_{16} - H_{28}$) and III ($N_{15} - H_{24}$) are 4.379 kcal/mol, 10.818 kcal/mol and 5.572 kcal/mol respectively. In these interactions, two interactions 4HBH ($N_{15} - H_7$) and III ($N_{15} - H_{24}$) are very weak as ($E_{int} < 5$ kcal/mol). Another two intreaction II ($N_{16} - H_{28}$) and III ($N_{16} - H_{18}$) are also weak intreaction as ($5 < E_{int} < 12$; in kcal/mol) [82].

3. Conclusion

We have designed and performed the DFT based calculations on 4-Hydroxy Benzo Hydrazide (4-HBH) and its derivatives (isomers I, II and III) with B3LYP/6-311 G (d, p) basis set. As 4-HBH and its derivatives (isomers I, II and III) are found to be potential pharmaceutically active, so we have focused our discussion mainly on vibrational, electronic and docking studies. On the basis of our calculations, we can conclude that, the addition of five membered ring to make new structures in 4-HBH structure tends to affect structural parameters of 4-HBH due to steric effects. The addition of five membered ring tends to increase the reactivity of molecules. Compound I is found to be more reactive than others due to its small energy gap between HOMO and LUMO. Chemical hardness (softness) value of compound I is lesser (greater) among all. Thus the compound (I) is found to be more reactive than all supported by hardness/ softness values too. The vibrational properties are also affected remarkably with the addition of five membered ring. In the absence of experimental IR spectra, we have reported theoretical vibrational spectra of all these compounds as this data is beneficial for the experimental researchers in near future. Therefore, the reported information should be reliable for future investigations. QATIM analysis shows that hydrogen bonding occurs in 4HBH, isomer II and III respectively. The most favourable binding occurs in isomer II by 6LU7 protease however most unfavourable binding occurs in between 4HBH and 6LU7 protease. From the above discussions in molecular docking section, we can say that 4-HBH and its derivatives (I, II, & III) may have good potential for treatment of COVID19. Therefore, we suggest quick clinical trials with 4-HBH and its derivatives (I, II, & III). Further studies are still in progress.

Acknowledgment

*This research is dedicated to all the volunteers from all over the world, who are serving against the COVID-19.

References

[1] Update on the prevalence and control of novel coronavirus-induced pneumonia as of 24:00 on February 21. http://www.nhc.gov.cn/xcs/yqtb/202002/543cc508978a48d2b9322bdc83daa6fd.shtml (accessed February 23, 2020).
[2] http://aajtak.indiatoday.in (31, March 2020).
[3] Guidelines for the Prevention, Diagnosis, and Treatment of Novel Coronavirus-induced Pneumonia, *The 6th ed.* http://www.nhc.gov.cn/yzygj/s7653p/202002/8334a8326dd94d329df351d7da8aefc2/files/b218cfeb1bc54639af227f922bf6b817.pdf (accessed February 23, 2020).
[4] U. Ashiq, R. Ara, M. Mahroof–Tahir, Z.T. Maqsood, K.M. Khan, S.N. Khan, H Siddiqui and M.I. Choudhary, *Chem Biodivers* **5**(1) (2008), 82.
[5] R. Ara, U. Ashiq, M. Mahroof-Tahir, Z.T. Maqsood, K.M. Khan, M.A. Lodhi and M.I. Choudhary, *Chem Biodivers* **4** (2007), 58.
[6] Z.T. Maqsood, K.M. Khan, U. Ashiq, R.A. Jamal, Z.H. Chohan, M. Mahroof– Tahir and C.T. Supuran, *J Enz Inhib Med Chem* **21** (2006), 37.
[7] K.S. Markley, *Fatty Acids, their Chemistry, Properties and Uses, InterScience Publishers*, New York, 1964. pp. 1604.
[8] I. Mir, M.T. Siddiqui and A. Comrie, *Tetrahedron* **26** (1970), 5235.
[9] E. Degener, H. Scheinplug and H.G. Schemelzer, *Brit Patent No.: 1035474*, 1967.
[10] R. Cavier and R. Rips, *J Med Chem* **8** (1965), 706.
[11] D.A. Raval and S.D. Toliwal, *J Oil Tech Assoc India* **26** (1994), 27.
[12] Abdulaziz A. Al-Saadi, *Journal of Molecular Structure* **1023** (2012), 115.
[13] D.M. Suresh, D. Sajan, Yun-Peng Diao, I. Nemec, I. Hubert Joe and V. Bena Jothy, *Spectrochimica Acta Part A: Molecular and Biomolecular Spectroscopy* **110** (2013), 157.
[14] H. Saleem, S. Subashchandrabose, N. Ramesh Babu and M. Syed Ali Padusha, *Spectrochimica Acta Part A: Molecular and Biomolecular Spectroscopy* **143** (2015), 230.
[15] K.K. Vijayaraj, B. Narayana, B.V. Ashalatha, N. Suchetha Kumari and B.K. Sarojini, *Eur J Med Chem* **42** (2007), 425.
[16] A.H. Abadi, A.A.H. Eissa and G.S. Hassan, *Chem Pharm Bull* **51** (2003), 838.
[17] C.G. Bonde and N.J. Gaikwad, *Bioorg Med Chem* **12** (2004), 2151.
[18] S.V. Bhandari, A.A. Patil, V. Sarkate, S.G. Gore and K.G. Bothra, *Bioorg Med Chem* **17** (2009), 390.
[19] K. Sugano, H. Hamada, M. Machida and H. Ushio, *J Biomol Screen* **6** (2001), 189.
[20] D.M. Suresh, D. Sajan, Yun-Peng Diao, I. Nemec, I. Hubert Joe and V. Bena Jothy, *Spectrochimica Acta Part A: Molecular and Biomolecular Spectroscopy* **110** (2013), 157.
[21] V. Arjunan, T. Rani, C.V. Mythili and S. Mohan, *Spectrochimica Acta Part A* **79** (2011), 486.
[22] Marta Sánchez-Lozano, Ezequiel M. Vázquez-López, José M. HermidaRamón and Carlos M. Estévez, *Polyhedron* **30** (2011), 953.
[23] M.K. Bharty, R.K. Dani, S.K. Kushawaha, Om Prakash, Ranjan K. Singh, V.K. Sharma, R.N. Kharwarc and N.K. Singh, *Spectrochimica Acta Part A: Molecular and Biomolecular Spectroscopy* **145** (2015), 98.
[24] A. Dwivedi, A.K. Srivastava and A. Bajpai, *Spectrochimicaacta part A: molecular and biomoleculat spectroscopy* **149** (2015), 343.
[25] A. Dwivedi, A.K. Pandey and N. Misra, *Spectroscopy: An International Journal* **27(3)** (2012), 155.
[26] A. Dwivedi, A.K. Pandey and N. Misra, *Spectroscopy: An International Journal* **26** (2011), 367.
[27] A.K. Pandey, A. Dwivedi and N. Misra, *Spectroscopy: An International Journal*, Volume 2013 (2013): Article ID 937915, pp. 11.
[28] A. Dwivedi and A. Kumar, Polycyclic Aromatic Compounds, 2019, https://doi.org/10.1080/10406638.2019.1591466.
[29] V. Arjunan et al., *Spectrochimica Acta Part A* **79** (2011), 486–496.
[30] S.S. Gupta, A. Marchno, R.D. Pradhan, C.F. Desai and J. Melikechi, *J Appl Phys* **89** (2001), 4939.
[31] S.P. Karna, *J Phys Chem A* **104** (2000), 4671.
[32] M.J. Frisch, G.W. Trucks, H.B. Schlegel, et al., Gaussian 03. Wallingford (CT): Gaussian Inc.; 2003.
[33] E. Frisch, H.P. Hratchian, R.D. Dennington II, et al., Gaussian Inc., GaussView. 2003.
[34] A.D. Becke, *J Chem Phys* **98** (1993), 5648.
[35] C. Lee, W. Yang and R.G. Parr, *Phys Rev B* **37** (1988), 785.
[36] Y. Tawada, T. Tsuneda, S. Yanagisawa, et al., *J Chem Phys* **120** (2004), 8425.
[37] H. Ar., T. Ozpozan, Z. Büyükmumcu, et al., *J Mol Struct* **1122** (2016), 48.
[38] M.H. Jamroz, "Vibrational Energy Distribution Analysis; VEDA4 Program," *SpectroChimica Acta A* **114** (2013), 220.
[39] https://www.chemcraftprog.com
[40] D.A. Kleinman, *Phys Rev* **126** (1962), 1977.
[41] J. Pipek and P.Z. Mezey, *J Chem Phys* **90** (1989), 4916.

[42] G. Mahmoudi, S. Rostamnia, G. Zaragoza, I. Brito, J. Cisterna and A. Cardenas, *J Chil Chem Soc* **64**(3) 2019.
[43] L.J. Bellamy, *The Infrared Spectra of Complex Molecules, third ed.,* Wiley, New York, 1975.
[44] R.M. Silverstein, G.C. Bassler and T.C. Morrill, *Spectrometric Identification of Organic Compounds fifth ed*., JohnWiley & Sons, Inc., New York, 1981.
[45] V. Arjunan, S. Mohan, S. Subramanian and B. Thimme Gowda, *Spectrochim Acta* **60A** (2004), 114.
[46] G. Varsanyi, *Assignments for Vibrational Spectra of Seven Hundred Benzene Derivatives, vol. I,* Adam Hilger, London, 1974.
[47] K.C. Chou, *Biophysical Journal* **45**(5) (1984), 881.
[48] H. Frohlich, Biological Coherence and Response to External Stimuli, Springer, Berlin, Germany, 1988.
[49] V. Arjunan, A. Jayaprakash, K. Carthigyan, S. Periandy and S. Mohan, *Spectro chim acta A* **108** (2013), 100-114.
[50] M. Gutowski and G. Chalasinski, *J Chem Phys* **98** (1993), 4540.
[51] S.C. Bose, H. Saleem, Y. Erdogdu, G. Rajarajan and V. Thanikachalam, *Spectrochim. Acta part A* **82** (2011), 260.
[52] J.S. Murray and K. Sen, *Molecular electrostatic potentials, Concepts and Applications* Elsevier Amsterdam 1996.
[53] D.A. Kleinman, *Phys, Rev B* **126** (1977), 1962.
[54] J. Pipek and P.J. Mezey, *J Chem Phys* **90** (1989), 4916.
[55] Y. Erdogdu, O. Unsalan and M.T. Gulluoglu, "FT-Raman, FT-IR spectral and DFT studies on 6, 8- dichloroflavone and 6, 8-dibromoflavone", *J Raman Spectrosc* **41** (2010), 820.
[56] Y. Erdogdu, O. Unsalan, M. Amalanathan and J.I. Hubert, *J Mol Struct* **980** (2010), 24.
[57] N. Gonohe, H. Abe, N. Mikami and M. Ito, *J Phys Chem* **89** (1985), 3642.
[58] L.A. Flippin, D.W. Gallagher and K. Jalali-Araghi, *J Org Chem* **54** (1989), 1430.
[59] R.G. Parr, L.V. Szentpály and S. Liu, *J Am Chem Soc* **121** (1999), 1922.
[60] P.K. Chattaraj and S. Giri, *J Phys Chem A* **111** (2007), 11116.
[61] J. Padmanabhan, R. Parthasarathi, Subramaniaan and P.K. Chattaraj, *J Phys Chem A* **111** (2007), 1358.
[62] P.W. Ayers and R.G. Parr, *J Am ChemSoc* **122** (2000), 2010.
[63] W.L. Jorgensen and E.M. Duffy, *Bioorg Med Chem Lett* **10** (2000), 1155.
[64] J.J. Huuskonen, D.J. Livingstone and I.V. Tetko, *J Chem Inf Comput Sci* **40**(4) (2000), 947.
[65] I.V. Tetk, V.Y. Tanchuk, T.A. Kasheva and A.E. Villa, *J Chem Inf Comput Sci* **41** (2001), 1488.
[66] I.V. Tetk, V.Y. Tanchuk, T.A. Kasheva and A.E. Villa, *J Chem Inf Comput Sci* **41** (2001), 1407–21.
[67] I.V. Tetko, V.Y. Tanchuk, T.N. Kasheva and A.E.P. Villa, *J Chem Inf Comput Sci* **41** (2001), 246.
[68] http://www.swissdock.ch
[69] http://www.rcsb.org/structure/6LU7 (accessed on 14 March 2020).
[70] I.F. Matta and R.J. Boyd, Wiley-VCH Verlag Gmbh, 2007.
[71] U. Koch and P. Popelier, *J Phys Chem A* **99** (1995), 9747–9754.
[72] R.F.W. Bader, Atoms in Molecules: A Quantum Theory (2nd edn) 1990 (Oxford: New York, NY.
[73] D. Cremer, E. Kraka, *Croat Chem Acta* **57** (1984), 1259, 5B. D. Cremer, E. Kraka, Angew. Chem., *Int Ed Engl* **23** (1984), 627. doi:10.1002/ANIE.198406271
[74] R.G.A. Bone, R.F.W. Bader, *J Phys Chem A* **100** (1996), 10892. doi:10.1021/JP953512M,
[75] M.F. Bobrov, G.V. Popova and V.G. Tsirelson, *Russ J Phys Chem* **80** (2006), 584. doi:10.1134/S0036024406040182
[76] P. Macchi and A. Sironi, *Coord Chem Rev* (2003), 238–239, 382.
[77] E. Espinosa, I. Alkorta, J. Elguero and E. Molins, *J Chem Phys* **117** (2002), 5529.
[78] R.F.W. Bader, *Atoms in Molecules: A Quantum Theory* (2nd edn) n1990 (Oxford: New York, NY.
[79] R.F.W. Bader and H. Esse´n, *J Chem Phys* **80** (1984), 1943. doi:10.1063/1.446956.
[80] S. Jenkins and I. Morrison, *Chem Phys Lett* **317** (2000), 97.
[81] E. Espinosa, E. Molins and C. Lecomte, *Chem Phys Lett* **285** (1998), 170–173.
[82] I. Rozas, I. Alkorta and J. Elguero, *J Am Chem Soc* **122** (2000), 11154–11161.